Journal of Alloys and Compounds 586 (2014) 611–615

Contents lists available at ScienceDirect

Journal of Alloys and Compounds

journal homepage: www.elsevier.com/locate/jalcom

A hybrid functional study of the electronic and optical properties of tetragonal PbO-type phase of ZnO under pressure

Qingbo Wang [a,b], Yanwei Wen [a], Rong Chen [c,*], Bin Shan [a,d,*]

[a] State Key Laboratory of Material Processing and Die and Mould Technology and School of Materials Science and Engineering, Huazhong University of Science and Technology, Wuhan 430074, Hubei, People's Republic of China
[b] School of Mathematics and Physics, China University of Geosciences (Wuhan), Wuhan 430074, Hubei, People's Republic of China
[c] State Key Laboratory of Digital Manufacturing Equipment and Technology and School of Mechanical Science and Engineering, Huazhong University of Science and Technology, Wuhan 430074, Hubei, People's Republic of China
[d] Department of Materials Science and Engineering, The University of Texas at Dallas, Richardson, TX 75080, USA

ARTICLE INFO

Article history:
Received 6 September 2013
Received in revised form 12 October 2013
Accepted 16 October 2013
Available online 28 October 2013

Keywords:
B10 phase ZnO
First principles
Hybrid functional theory
Pressure
Electronic and optical properties

ABSTRACT

To extend our knowledge on the tetragonal PbO-type (*B*10) phase of ZnO under high pressure, we used the hybrid functional theory to calculate its electronic and optical properties. Our calculations indicate that the *B*10 phase is a transparent insulator and has an indirect band gap ranging from 6.08 to 7.06 eV with pressure increasing from 236 to 316 GPa. The *B*10 phase under 236 GPa has excellent dielectric properties except metallic behaviors at around 25 and 37 eV photon excitation. We found a blue shift in optical properties of the *B*10 phase with the increase of pressure.

1. Introduction

ZnO is an important semiconductor, optical material as well as a mineral in the lower mantle. ZnO crystallizes in wurtzite (*B*4) phase at ambient pressures and has many industrial applications [1–3], such as nanolasers, photodetectors, liquid crystal displays, transparent conductive films and light-emitting diodes. With the development of high-pressure equipment and advances in computational methods, more and more efforts have been devoted to the studying of materials under pressure [4–7] as well as their applications [8–12].

A number of experimental studies have been conducted to study phase transitions of ZnO under pressure by high-pressure equipment. The X-ray spectrum technique is commonly used to determine the transition pressure between *B*4 and *B*1 phases of ZnO upon increasing-pressure [13–15]. Mossbauer spectroscopy is another useful technique to detect the lattice soft modes and nonaxial lattice distortions of ZnO, which can be used to infer the phase transition of ZnO [14]. Desgreniers et al. found experimentally that ZnO could transform from wurtzite (*B*4) phase to rock salt (*B*1) phase under 9.1 GPa by synchrotron radiation [13]. Karzel et al. reported evidences of *B*4–*B*1 transition at 8.7 GPa by X-ray and Zn-67-Mossbauer spectroscopy [14]. Liu et al. proposed that ZnO could *B*1 phase's stability all the way up to 209 GPa using synchrotron X-ray diffraction method [15]. Corresponding theoretical calculations had also been carried out to investigate different phases of ZnO such as *B*1, *B*2, *B*3 and *B*4 phases [16,17]. It was found that the *B*3 phase is not stable and phase transitions among those phases under high pressure is from *B*4 to *B*1 to *B*2 with transition pressures of 8.8 GPa and 263 GPa, respectively. It was also predicted that the bandgap of *B*4 is direct while the other two are indirect [17]. On the other hand, the *B*4–*B*1 transition has also been investigated by first-principles calculations and the calculated transition pressure agrees well with the experimental data. Another phase transition (*B*1 to CsCl (*B*2) phase) has also been predicted to be around 263 GPa.

Recently, Li et al. theoretically predicted the existence of a PbO-type (*B*10) phase of ZnO between 236 and 316 GPa [18]. Pu et al. further investigated the optical properties of *B*10 phase ZnO under 250 GPa using a GGA-PBE method [19]. However, due to limitation in experimental operating conditions (the highest available pressure $\leqslant$209 GPa) [15], the *B*10 phase of ZnO have not been obtained experimentally. Lack of experimental data makes it harder to

* Corresponding authors. Address: State Key Laboratory of Material Processing and Die and Mould Technology and School of Materials Science and Engineering, Huazhong University of Science and Technology, Wuhan 430074, Hubei, People's Republic of China. Tel.: +86 18971547499 (B. Shan).
E-mail addresses: rongchen@mail.hust.edu.cn (R. Chen), bshan@mail.hust.edu.cn (B. Shan).

0925-8388/$ - see front matter © 2013 Elsevier B.V. All rights reserved.
http://dx.doi.org/10.1016/j.jallcom.2013.10.127

understand the electronic and optical properties of the *B*10 phase. Fortunately, first-principles methods especially the recent advances in hybrid functional calculations, provide us an effective approach to reliably predict the electronic and optical properties of the high pressure *B*10 phase ZnO.

ZnO is a strongly correlated material and the localized electrons in ZnO have strong coulombic interactions. Standard GGA-PBE [20] method usually fails reproducing the correct band gap. The hybrid functional method, on the other hand, can remedy this problem and predict the electronic structure and band gap of ZnO with much higher accuracy and reliability [21–23]. In the present work, hybrid functional method is used to investigate the structural, electronic and optical properties of the *B*10 phase ZnO. The changes of such properties under high-pressure conditions were also calculated and discussed. We found that the imaginary and real part of the complex dielectric function shifted to higher energy with increasing pressure. Five main peaks of the imaginary part of dielectric function were found around 12.8, 16.3, 22.0, 26.2 and 34.3 eV at a pressure between 236 and 316 GPa. These peaks locate in the shortwave region which may facilitate the use of ZnO B10 phase in certain optical devices. Our researches extend the knowledge about electronic and optical properties of the *B*10 phase ZnO.

2. Computational method

Our calculations were performed by VASP software based on density functional theory. The crystal structure was first optimized using GGA–PAW method, followed by a static Heyd–Scuseria–Ernzerhof (HSE) functional calculation to get the electronic and optical properties. We used an energy cutoff of 600 eV and $8 \times 8 \times 11$ Monkhorst–Pack grids [24] to sample the first Brillouin zone which were tested to yield good convergence. The valence electron configurations of Zn and O used in our calculations were $3d^{10}4s^2$ and $2s^22p^4$, respectively. The band gap with the HSE hybrid functional can be conceptually divided into two contributions:

$$E^{\text{hybrid}} = \alpha E^{\text{Fock}} + (1-\alpha)E^{\text{GGA}} \quad (1)$$

where the first contribution arises from the Hartree–Fock exact exchange and the second term is from standard GGA. It has been reported that an α value of 0.375 would be suitable for ZnO [25]. We thus adopt $\alpha = 0.375$ in our calculations. The calculated band gap of wurtzite phase ZnO is 3.31 eV, which agrees reasonably well with the experimental value (3.44 eV) [26]. Considering the anisotropic nature of *B*10 phase crystal, we used polycrystalline polarization in our optical calculations for simplicity.

3. Results and discussion

3.1. Band structure

The *B*10 phase ZnO has a PbO-type structure, which belongs to the P4/nmm space group. Zn^{2+} and O^{2-} ions stack in layers in the crystal alternatively. The optimized lattice constants at 250 GPa are $a = b = 3.241$ Å and $c = 2.291$ Å, which agrees well with previous studies [18,19]. We calculated the band structures of the *B*10 phase under different pressures (236,270,290 and 316 GPa). The band structure at 236 and 316 GPa are shown in Fig. 1a as a representive example. It can be seen from the figure that the conduction band minimum and the valence band maximum appear at Γ and *M* points, respectively. Thus the *B*10 phase is predicted to be an indirect band gap semiconductor, which is consistent with previous results from GGA-PBE [18,19].

We note the profiles of the band structure of *B*10 phase ZnO under different pressures are topologically similar. Fig. 1a shows the valence band is flat around the Fermi level. The flat Fermi level indicates relatively heavy holes in the *B*10 phase. As the pressure increases, the conduction and valence band shift to higher and lower energies, respectively. The shifts of the conduction and valence band result in an increasing band gap. Fig. 1a shows the band gap of the *B*10 phase under 236 and 316 GPa are 6.08 and 7.06 eV respectively, which is nearly twice that of wurtzite phase (3.44 eV). The wide band gap implies that *B*10 phase ZnO has potential optical applications in the shortwave region and in high-temperature conditions. The pressure dependence of the band gap is shown in Fig. 1b, clearly indicating the enlargement of the band gap with the increasing pressure. The increased band gap shows *B*10 phase ZnO becomes more dielectric. And a nearly linear relationship is found between the band gap and the pressure.

3.2. Electronic density of states and the dielectric function

The total density of states (DOS) and partial density of states (PDOS) of the *B*10 phase ZnO under 236 and 316 GPa are shown in Fig. 2. A slight shift of the peaks of DOS for conduction and valence bands are expanded to higher and lower energy range. And the expansions are consistent with the band structures. According to the PDOS, the valence bands near the Fermi level (−5.4 to −2.5 eV) mainly come from O 2*p* and Zn 3*d* states and a strong hybridization can be found between Zn 3*d* state and the O 2*p* state in the valence band. The conduction band minimum is mainly composed of Zn 4*s* and O 2*p* states. The valence band (−7.1 to −5.4 eV) derives from O 2*p* and Zn 3*d* states. The band energy between (−14.2 to −7.1 eV) mainly comes from Zn 3*d*, while O 2*p* contributes little in this energy range.

We used the complex dielectric function $\varepsilon(\omega) = \varepsilon_1(\omega) + i\varepsilon_2(\omega)$ to describe the response of *B*10 phase ZnO to photon excitation. The imaginary part ($\varepsilon_2(\omega)$) of the dielectric function is an important parameter in the optical properties. The calculations of ε_2 are based on the momentum matrix elements, which are related to the electronic transitions between occupied and unoccupied wave functions. The functions also obey the selection rule. We first calculated the ε_2 (Eq. (2)) of the *B*10 phase and then used the Kramer–Kronig relation (Eq. (3)) to calculate the real part ($\varepsilon_1(\omega)$) of ε.

$$\varepsilon_2(\omega) = \frac{2e^2\pi}{\Omega\varepsilon_0}\sum_{k,v,c}|\langle\psi_k^c|\hat{u}\cdot r|\psi_k^v\rangle|\delta(E_k^c - E_k^v - E) \quad (2)$$

$$\varepsilon_1 = 1 + \frac{2}{\pi}p\int_0^\infty \frac{\omega'\varepsilon_2(\omega')}{\omega'^2 - \omega^2}d\omega' \quad (3)$$

In Eq. (2), the superscript *c* and *v* mean conduction and valence bands, respectively. In Eq. (3), *p* is the principal value of the integral. The dielectric function of *B*10 phase under 236, 270, 290 and 316 GPa are calculated with photon energy from 0 to 60 eV in Fig. 3a. It shows that ε_2 starts at 9.8, 10.1 and 10.5 eV for the *B*10 phase at 236, 270 and 316 GPa, respectively. The threshold energies are larger than the band gaps (6.08, 6.59 or 7.06 eV). It is reasonable since the *B*10 phase is an indirect band gap insulator. The threshold energy is estimated to be the direct transition at Γ point. We notice there are five main peaks under each pressure in this photon energy range. For example, with the pressure increases from 236 to 316 GPa, the peaks at 12.4, 15.8, 21.7, 25.8 and 33.9 eV shift to 13.3, 16.6, 22.4, 26.7 and 34.8 eV respectively. The energy shifts are from 0.7 to 0.9 eV. Moreover, the peaks of ε_2 shift to higher energy as the pressure increases. The related ε_1 are calculated in Fig. 3b and the peaks of ε_1 follow a similar trend of ε_2 when applying an increasing pressure on *B*10 phase ZnO. When the pressure increases from 236 to 316 GPa, negligible change of ε_1 can be found in the energy range less than 7 eV and it is predicted the *B*10 phase of ZnO exhibit an excellent dielectric behavior. Interestingly, there are two broad peaks around 25 and 37 eV below zero, which indicates the *B*10 phase may show metallic behavior at such photon energy.

Since the imaginary part (ε_2) is closely related to the electronic transition between energy bands, we will focus on this in the following discussions. The peaks around 13 eV corresponds to the

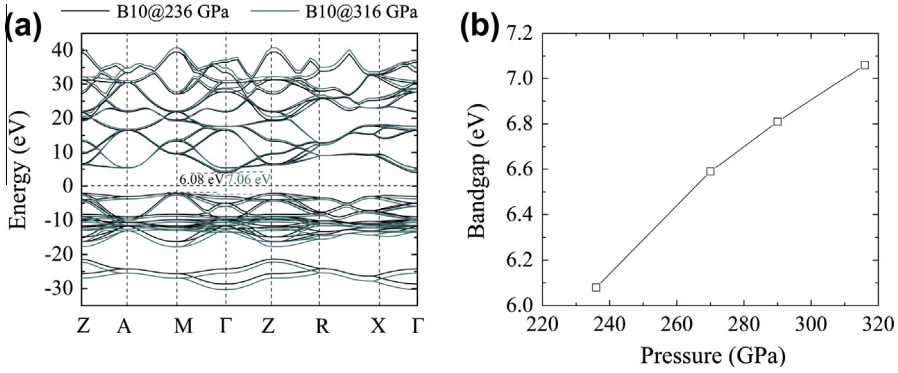

Fig. 1. (a) The band structures of the *B*10 phase of ZnO at 236 and 316 GPa; (b) the dependence of the band gap of the *B*10 phase of ZnO on pressure.

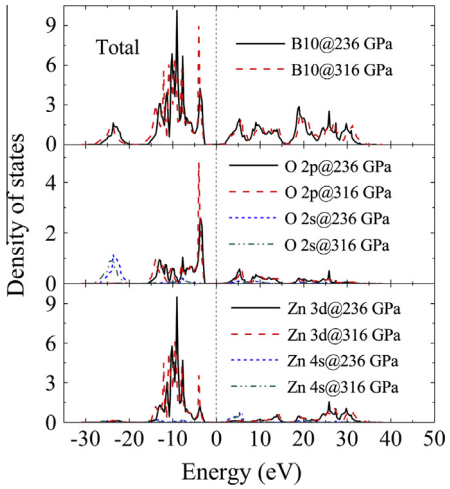

Fig. 2. The total and partial densities of states of the *B*10 phase of ZnO at 236 and 316 GPa.

transition between O 2*p* (top of the valence band) and Zn 4*s* states (bottom of the conduction band). The peaks around 16 eV come from the transition between Zn 3*d* and O 2*p* states. The peaks around 22 and 26 eV arise from the electrons transition between Zn 3*d* and O 2*s*. The peaks around 34 eV come from the transition between deep valence bands and conduction bands. The intensity of the peaks around 26 and 34 eV is less than other three peaks since the transitions at high energy are rare. These transitions are in line with other reports [27,28]. The five main peaks indicate the *B*10 phase can be used as optical devices in a shortwave region.

3.3. Optical constants

Optical constants are important in designing optical devices. As *B*10 phase has tetragonal symmetry, its optical constants show anisotropy. For simplicity, we consider the optical constants of the polycrystalline *B*10 phase ZnO. We used the following Eqs. (4)–(7) [29,30] when calculating the relevant optical constants:

$$R(\omega) = \left| \frac{\sqrt{\varepsilon_1(\omega) + j\varepsilon_2(\omega)} - 1}{\sqrt{\varepsilon_1(\omega) + j\varepsilon_2(\omega)} + 1} \right|^2 \tag{4}$$

$$\alpha(\omega) = \sqrt{2}\omega \left[\sqrt{\varepsilon_1^2(\omega) + \varepsilon_2^2(\omega)} - \varepsilon_1(\omega) \right]^{1/2} \tag{5}$$

$$n(\omega) = \left[\sqrt{\varepsilon_1^2(\omega) + \varepsilon_2^2(\omega)} + \varepsilon_1(\omega) \right]^{1/2} \Big/ \sqrt{2} \tag{6}$$

$$L(\omega) = \frac{\varepsilon_2(\omega)}{\varepsilon_1^2(\omega) + \varepsilon_2^2(\omega)} \tag{7}$$

Fig. 4 shows the reflectivity ($R(\omega)$), absorption coefficient ($\alpha(\omega)$), real part of the refractive index ($n(\omega)$) and electron energy-loss functions ($L(\omega)$) at 236, 270 and 316 GPa with photon energy ranging from 0 to 60 eV. These calculated constants can help us to identify the *B*10 phase under high pressures. From Fig. 4, we can see that peaks of optical constants shift to higher energies with increasing pressure (blue shift). We take $\alpha(\omega)$ in Fig. 4b as an example and the detail positions of peak A are shown in Fig. 4a. The dependence of the position of peak A on pressure is almost linear as shown in Fig. 4d. The relationship between position energy

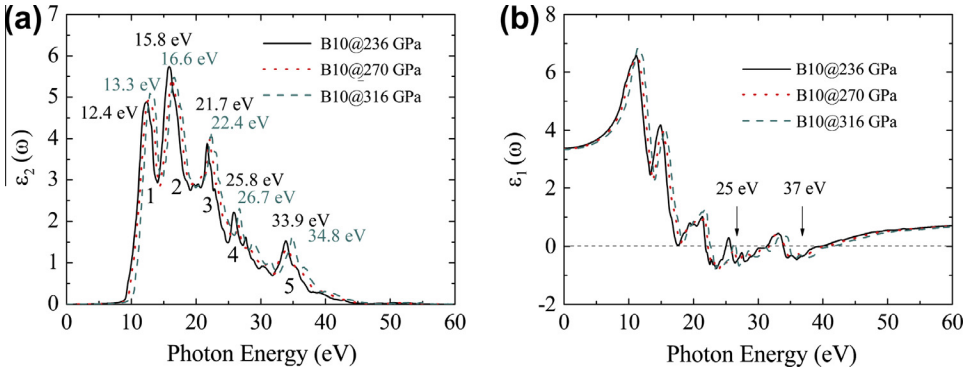

Fig. 3. The dependence of the complex dielectric function of the *B*10 phase of ZnO on photon energy at 236, 270 and 316 GPa: (a) the imaginary part ($\varepsilon_2(\omega)$) and (b) the real part ($\varepsilon_1(\omega)$).

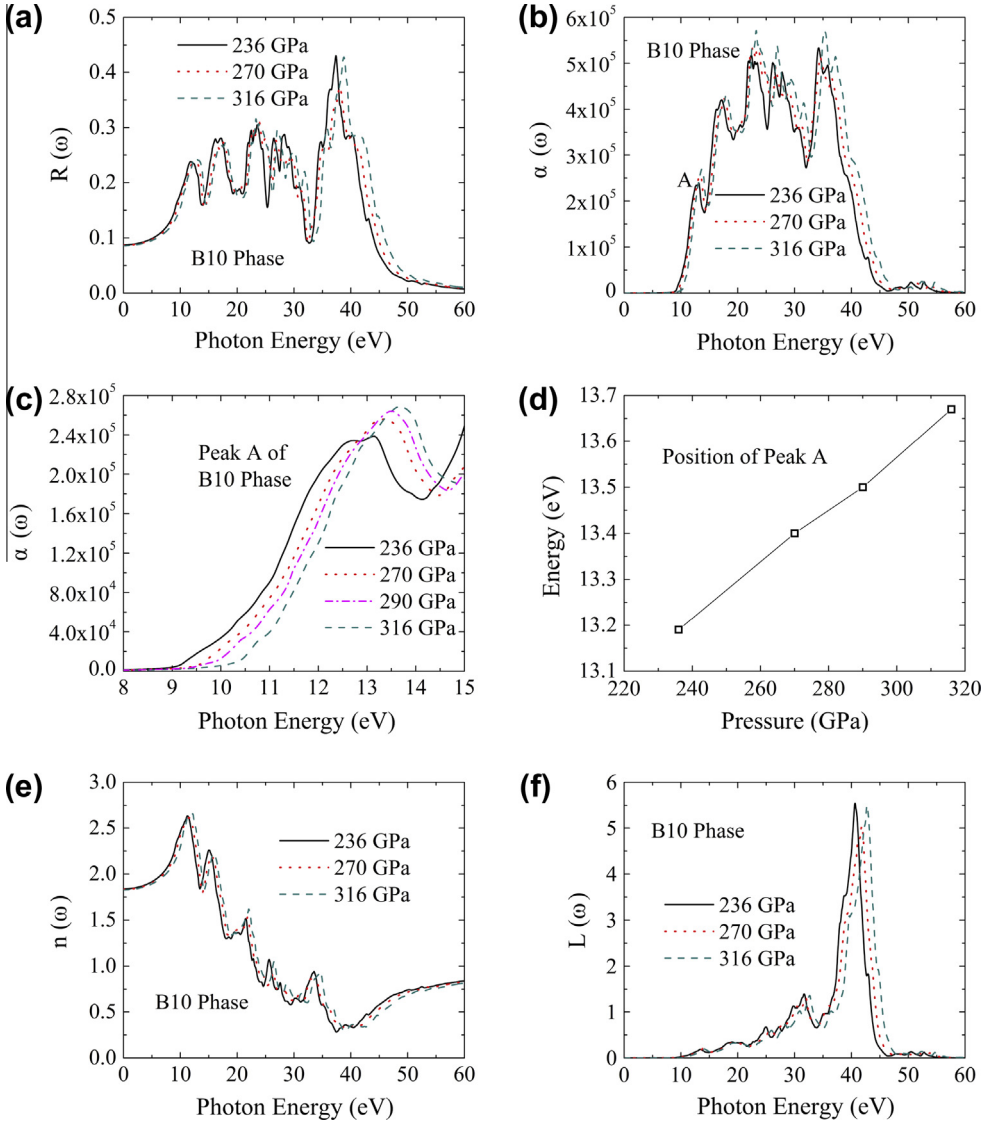

Fig. 4. The optical constants of *B*10 phase of ZnO: (a) reflectivity ($R(\omega)$); (b) absorption coefficient ($\alpha(\omega)$); (c) peak A of $\alpha(\omega)$ between 8 and 15 GPa; (d) position of peak A between 236 and 316 GPa; (e) the real part of the refractive index ($n(\omega)$) and (f) electron energy-loss functions ($L(\omega)$).

(E_A) and pressure (P) can be described by $E_A = 11.79 + 0.00594P$. In the equation, the unit of the E_A and P is eV and GPa. The linear-dependence relationship between E_A and P of these constants can be used to measure pressure after carefully calibrated.

Among these constants, $L(\omega)$ is an important optical constant, as it represents a fast electron energy loss when an electron crosses a crystal. The peaks of $L(\omega)$ are closely related to plasma resonance and arise from the trailing edges of $R(\omega)$. For example, the peaks of $L(\omega)$ around 31 and 41 eV arise from the abrupt reduction of $R(\omega)$. $R(\omega)$ remains almost constant at 0.09 when energy range is from 0 to 5.3 eV and $n(\omega)$ is 1.9 in the energy range from 0 to 6.7 eV. We note the pressure has little effect on the $n(0)$ and $R(0)$. Fig. 4e and f shows the $\alpha(\omega)$ and $L(\omega)$ show appreciable values starting from 10.3 eV. The constant n and started energy of α and L indicate the *B*10 phase is a transparent crystal.

The optical band gap can be calculated according to the equation $\alpha h\nu = c(h\nu - E_g')^{1/2}$, where α is the absorption coefficient, h denotes the Planck constant, ν indicates the frequency, c denotes a constant, and E_g' is the optical band gap. Since the relationship between $(\alpha h\nu)^2$ and $h\nu$ is linear, E_g' can be determined from the intercept. We see that the E_g' increased from 10.9 to 10.7 eV with pressure increased from 236 to 316 GPa. As the pressure increases, the widening value (0.8 eV) of the optical band gap is close to the widening value of the band gap (0.98 eV). The values of the optical band gap are nearly 1.7 times to those of the electronic band gap. The optical band gap of *B*10 phase ZnO might be verified by optical method [31] in the future.

4. Conclusions

To extend our knowledge about the *B*10 phase ZnO under pressure, we used the hybrid functional method to study its electronic and optical properties. We found the band gap enlarges with increasing pressure. The dielectric functions were calculated and the peaks of ε_2 and ε_1 shifted to higher energy with increasing pressure. The relationship between the peaks and the electronic transition in the *B*10 phase was discussed. By utilizing the linear-dependence relationship between the positions of the peaks and pressures, it can be used to measure the pressure after careful calibration. Our study help clarify some basic properties of the *B*10 phase under high pressure and benefits future experiments in this field.

Acknowledgments

This work is supported by the National Basic Research Program of China (2013CB934800 and 2011CB606401), the National Natural Science Foundation of China (41104054), Fundamental Research Funds for the Central Universities, HUST (2012TS012 and 2012TS076) and China Postdoctoral Science Foundation (2012M521421). The authors thank the Texas Advanced Computing Center (TACC) at The University of Texas at Austin (http://www.tacc.utexas.edu) for providing grid resources that have contributed to the research results reported within this paper.

References

[1] J. Serrano, A.H. Romero, F.J. Manjón, R. Lauck, M. Cardona, A. Rubio, Phys. Rev. B 69 (2004) 094306.
[2] J.E. Jaffe, J.A. Snyder, Z.J. Lin, A.C. Hess, Phys. Rev. B 62 (2000) 1660–1665.
[3] U. Ozgur, Y.I. Alivov, C. Liu, A. Teke, M.A. Reshchikov, S. Dogan, V. Avrutin, S.J. Cho, H. Morkoc, J. Appl. Phys. 98 (2005) 041301.
[4] R.C. Liebermann, High Pressure Res. 31 (2011) 493–532.
[5] M.D. Segall, P.J.D. Lindan, M.J. Probert, C.J. Pickard, P.J. Hasnip, S.J. Clark, M.C. Payne, J. Phys. Condens. Matter 14 (2002) 2717–2744.
[6] P. Wang, Y. Cheng, X.H. Zhu, X.R. Chen, G.F. Ji, J. Alloys Comp. 526 (2012) 74–78.
[7] S. Agduk, G. Gokoglu, J. Alloys Comp. 520 (2012) 93–97.
[8] D. Errandonea, F.J. Manjon, Prog. Mater Sci. 53 (2008) 711–773.
[9] S. Adak, H. Nakotte, P.F. de Chatel, B. Kiefer, Physica B 406 (2011) 3342–3347.
[10] Y.L. Li, W.L. Fan, H.G. Sun, X.F. Cheng, P. Li, X. Zhao, J.C. Hao, M.H. Jiang, J. Phys. Chem. A 114 (2010) 1052–1059.
[11] G. Fadda, G. Zanzotto, L. Colombo, Phys. Rev. B 82 (2010) 064106.
[12] S. Aydin, M. Simsek, J. Alloys Comp. 509 (2011) 5219–5229.
[13] S. Desgreniers, Phys. Rev. B 58 (1998) 14102–14105.
[14] H. Karzel, W. Potzel, M. Köfferlein, W. Schiessl, M. Steiner, U. Hiller, G.M. Kalvius, D.W. Mitchell, T.P. Das, P. Blaha, K. Schwarz, M.P. Pasternak, Phys. Rev. B 53 (1996) 11425–11438.
[15] H.Z. Liu, J.S. Tse, H.K. Mao, J. Appl. Phys. 100 (2006) 093509.
[16] B. Amrani, I. Chiboub, S. Hiadsi, T. Benmessabih, N. Hamdadou, Solid State Commun. 137 (2006) 395–399.
[17] S. Cui, W. Feng, H. Hu, Z. Feng, Y. Wang, J. Alloys Comp. 476 (2009) 306–310.
[18] Z.W. Li, Y. Xu, G.Y. Gao, T. Cui, Y.M. Ma, Phys. Rev. B 79 (2009) 193201.
[19] C.Y. Pu, X. Tang, Q.Y. Zhang, Solid State Commun. 151 (2011) 1533–1536.
[20] J.P. Perdew, K. Burke, M. Ernzerhof, Phys. Rev. Lett. 77 (1996) 3865–3868.
[21] M. Ramzan, Y. Li, R. Chimata, R. Ahuja, Comput. Mater. Sci. 71 (2013) 19–24.
[22] L.X. Qin, Y.F. Duan, H.L. Shi, L.W. Shi, G. Tang, J. Phys. Condens. Matter. 25 (2013) 11.
[23] T. Kaewmaraya, M. Ramzan, H. Lofas, R. Ahuja, J. Appl. Phys. 113 (2013) 5.
[24] H.J. Monkhorst, J.D. Pack, Phys. Rev. B 13 (1976) 5188.
[25] F. Oba, M. Choi, A. Togo, A. Seko, I. Tanaka, J. Phys. Condens. Matter. 22 (2010) 384211.
[26] A. Mang, K. Reimann, S. Rübenacke, Solid State Commun. 94 (1995) 251–254.
[27] X.D. Zhang, M.L. Guo, W.X. Li, C.L. Liu, J. Appl. Phys. 103 (2008) 063721.
[28] J. Sun, H.T. Wang, J.L. He, Y.J. Tian, Phys. Rev. B 71 (2005) 125132.
[29] M.Q. Cai, Z. Yin, M.S. Zhang, Appl. Phys. Lett. 83 (2003) 2805–2807.
[30] S. Saha, T.P. Sinha, A. Mookerjee, Phys. Rev. B 62 (2000) 8828–8834.
[31] M. Lorenz, E.M. Kaidashev, A. Rahm, T. Nobis, J. Lenzner, G. Wagner, D. Spemann, H. Hochmuth, M. Grundmann, Appl. Phys. Lett. 86 (2005) 143113.